Archives of Academic Emergency Medicine. 2026; 14(1): e29

ORIGINAL RESEARCH

Nano-Formulated Apelin13 Reduces Cerebral Ischemia/Reperfusion Injury in Rats by Suppressing Activity of TLR4/MyD88/NF-κB Axis and Pro-inflammatory Cytokines; an Experimental Study

Elham Kashafi Jahromi[1], Solmaz Nasseri Maleki[2,3], Michael R Hamblin[4], Fatemeh Ramezani[3]*, Nahid Aboutaleb[1,3]†

1. Department of Physiology, School of Medicine, Iran University of Medical Sciences, Tehran, Iran.
2. Student Research Committee, Iran University of Medical Sciences, Tehran, Iran.
3. Physiology Research Center, Iran University of Medical Sciences, Tehran, Iran.
4. Laser Research Centre, Faculty of Health Science, University of Johannesburg, Doornfontein 2028, South Africa.

Received: May 2026; Accepted: June 2026; Published online: 25 July 2026

Abstract: **Introduction:** Nanocarrier-mediated delivery represents a promising strategy for enhancing the therapeutic efficacy of pharmacological agents. This study investigated whether encapsulating the endogenous peptide apelin-13 in niosomes (Nano-Apelin13) could improve its protective effects against ischemic stroke injury in rats. **Methods:** Transient focal cerebral ischemia was induced by 60-minute middle cerebral artery occlusion (MCAO) followed by 24-hour reperfusion. Sixty rats were randomly allocated into five experimental groups: Sham, CI/R (ischemia/reperfusion), CI/R + empty niosomes, CI/R + free Apelin13, and CI/R + Nano-Apelin13. Free Apelin13 and Nano-Apelin13 (40 µg/kg) were administered intravenously 1 hour after reperfusion onset. After 24 hours, cerebral infarction size, neurological deficit scores, brain water content, and neuronal damage were evaluated. Protein expression levels of TLR4, MyD88, NF-κB, TNF-, and IL-1β were analyzed by western blotting. **Results:** Both free Apelin13 and Nano-Apelin13 significantly reduced cerebral infarct volume, improved neurological scores, decreased neuronal loss, and downregulated MyD88 and NF-κB expression. However, Nano-Apelin13 demonstrated superior efficacy, normalizing several parameters to sham-operated levels. Notably, Nano-Apelin13 significantly suppressed TLR4 expression and attenuated cerebral edema and pro-inflammatory cytokine production, effects that were either significantly enhanced or absent in the free Apelin13-treated group.
Conclusion: Delivery of Apelin13 in niosomes could be a good option to reduce CI/R damage by inhibiting the activity of TLR4/MyD88/NF-kB axis compared to free Apelin13.

Keywords: Brain Ischemia; Apelin, Apelin-13 peptide; Drug Delivery Systems; Signal Transduction; Toll-Like Receptor 4; Myeloid Differentiation Factor 88

Cite this article as: Kashafi Jahromi E, Nasseri Maleki S, Hamblin MR, et al. Nano-Formulated Apelin13 Reduces Cerebral Ischemia/Reperfusion Injury in Rats by Suppressing Activity of TLR4/MyD88/NF-κB Axis and Pro-inflammatory Cytokines; an Experimental Study. Arch Acad Emerg Med. 2026; 14(1): e29. https://doi.org/10.22037/aaem.v14i1.2941.

1. Introduction

Ischemic stroke (IS) is caused by an embolus or thrombus blocking the cerebral arteries and depriving the brain of oxygen (Feske 2021). The neuronal cells in the core region of the brain affected by ischemia begin to undergo irreversible cell death within 8-10 minutes of the blood supply being blocked. This critical time represents the 'golden hour' for treatment, as neuronal cells in the ischemic core begin to undergo irreversible death once blood flow is interrupted beyond this timeframe, making immediate medical intervention essential to salvage viable brain tissue and prevent permanent neurological damage (Powers, Rabinstein et al. 2019). Due to the complex nature of IS, it is a major cause of long-term disability without any satisfactory treatment, and has a high rate of morbidity and mortality worldwide (Feigin, Stark et al. 2021). The mental and physical health of patients is strongly affected by IS which in turn increase the economic and social burden on society (Schneider, Taba et al. 2021). Although thrombolytic therapy administered within 4h following a stroke is the gold standard option to prevent damage (Yafasova, Fosbøl et al. 2021), reperfusion may then further increase the injury due to abnormal Ca2+ accumulation in

***Corresponding Author:** Fatemeh Ramezani; Physiology Research Center, Iran University of Medical Sciences, Tehran, Iran. E-mail: ramezani.f@iums.ac.ir, Tel: 09120929047. ORCID: https://orcid.org/0000-0002-8545-3521.
†**Corresponding Author:** Nahid Aboutaleb; Physiology Research Center, Iran University of Medical Sciences, Tehran, Iran. Email: aboutaleb.n@iums.ac.ir, Tel:09123856305, ORCIDs: https://orcid.org/0000-0002-7514-5939.

the mitochondria and generation of free radicals (Kleindorfer, Towfighi et al. 2021, Mendelson and Prabhakaran 2021). Several harmful cellular stresses such as glutamate excitotoxicity, inflammation, and oxidative stress are involved in the pathogenesis of IS damage via the activation or inactivation of various cellular pathways (Wang, Zhang et al. 2022, Wang, Pan et al. 2023). Among these cellular pathways, there is a mutual interaction between TLR4, MyD88 and the NF-κB transcription factor (Yang, Gong et al. 2021) . During ischemia, NF-κB translocates into the nucleus from the cytoplasm due to activation of TLR4/MyD88, and stimulates the production of pro-inflammatory cytokines (PCs) including TNF-, IL-1β, and IL-6 (Barton and Medzhitov 2003).

Apelin is a 77 amino acid endogenous peptide ligand for the G protein-coupled receptor APJ. Apelin13 is the main isoform in the human brain and heart, and is a key player in numerous normal physiological processes as well as pathophysiological responses like angiogenesis, neuroinflammation, and oxidative stress (Zhang, Jiang et al. 2023, Behrouzifar and Esmaily 2024). Despite reports of the neuroprotective effects of Apelin13, its short half-life in the bloodstream could be a limitation for clinical applications (Xu, Cui et al. 2022). To help solve this issue and increase Apelin13 efficiency, we could take advantage of the beneficial properties of niosomes, including biodegradability, low toxicity, capacity for loading both lipophilic and hydrophilic therapeutic agents, and controlled drug release (Riya, Dua et al. 2022). The current study tested whether encapsulation of Apelin-13 into niosomes could promote its efficacy for treating IS in rats.

2. Methods

2.1. Preparation of Nano-Apelin13

The Apelin 13 peptide was purchased from Santa Cruz (cod: sc171835, Santa Cruz, USA). Niosomes were prepared using the thin-layer hydration method. Firstly, surfactants (mixture of span60 and tween 60) and cholesterol at 1:1 molar ratio were dissolved in 10 mL chloroform. Chloroform was evaporated using a rotary evaporator at 60 °C and 120 rpm for 60 minutes. The dried thin film was hydrated with 10 mL of Apelin13 solution in PBS (60 mg/mL) under agitation at 120 rpm for 60 minutes at 30°C. The resulting Nano-Apelin13 suspension was sonicated for 5 min and stored at 4 °C.

2.2. Characterization of Apelin13-Loaded Niosomes

The Nano-Apelin13 niosomes were characterized using Dynamic Light Scattering (DLS) for size and polydispersity, zeta potential analysis for surface charge, Scanning Electron Microscopy (SEM) for morphological evaluation, and Fourier Transform Infrared Spectroscopy (FTIR) for chemical structure confirmation.

2.3. In Vitro Drug Release Study

In vitro drug release of Apelin13 from the niosomes was investigated using a dialysis method. The nanocomplex suspension was placed in a dialysis bag containing 10 mL of PBS (cellulose membrane, cutoff 12 kDa). The dialysis bag was immersed in 100 mL of PBS (pH 7.4) under magnetic stirring (37 °C, 150 rpm) for 24 h. At regular intervals, 2 mL of the release medium was withdrawn and the same volume of fresh PBS was replenished. The concentration of the released drug was measured at 296 nm using a UV-Vis spectrophotometer at predetermined time intervals. A calibration curve was constructed by measuring the absorbance of serial dilutions of Apelin13 at 296 nm.

2.4. Animals

All experiments and protocols were approved by the Animal Ethics Committee of the Iran University of Medical Sciences (IUMS) (IR.IUMS.FMD.REC.1402.083). 60 male Wistar rats (8 weeks old, 250–300 g) were provided by the animal laboratory of IUMS. The animals were housed in a 12 h light-dark schedule, 22 ± 1°C temperature, 45–55% humidity, with unrestricted access to standard food and water ad libitum.

2.5. MCAO/R model

The rats were anesthetized by ketamine (60mg/kg)/xylazine (5mg/kg) and received an incision on the middle region of neck skin. After separating the right common artery, ECA, and ICA, a 6-0 nylon monofilament was introduced into the right ICA until a slight resistance was felt, which confirmed successful occlusion. After 1 hour, the nylon monofilament was removed to re-establish blood circulation and then the agents were injected into the tail vein. Sham-operated animals were only exposed to incision of the skin and subcutaneous tissue without blocking the MCA.

2.6. Experimental Design and Blinding

Following MCAO induction, animals that met the inclusion criteria were randomly assigned to experimental groups using a computer-generated sequence. The rats were randomly assigned into five groups:

- Sham: surgery without MCAO
- CI/R: blocking MCA for 1 h and reperfusion for 24 h
- CI/R + Niosomes: blocking MCA for 1 h, i.v administration of only niosomes at 40 µg/kg and reperfusion for 24 h
- CI/R + Apelin13: blocking MCA for 1 h, i.v administration of free Apelin13 at 40 µg/kg and reperfusion for 24 h
- CI/R + Nano-Apelin13: blocking MCA for 60 min, i.v administration of nano-Apelin13 in a at 40 µg/kg and reperfusion for 24 h

All outcome assessments were performed by investigators blinded to the group allocation. The surgeon was blinded to treatment. Behavioral tests were video-recorded and scored by a blinded analyst. Infarct volume from coded TTC-stained images and protein expression from coded western blot images were quantified by blinded investigators using ImageJ

and densitometry, respectively.

2.7. Neurological severity score

A six-point scale described by Longa and coworkers was employed to measure neurological severity score (NSS) after 24 h (Longa, Weinstein et al. 1989): 0, no damage or impairment; 1, lack of ability to completely extend the contralateral forelimb; 2, lack of ability to extend the contralateral forelimb; 3, turning to the contralateral side; 4, collapsing to the left; 5, no spontaneous walking and a depressed state of consciousness.

2.8. Brain water content (BWC)

The animals were sacrificed and the brain samples removed from skull bone and the wet weight measured then, they were dried in a 37 °C incubator and the dry weight measured. BWC was calculated based on the formula (wet weight dry weight)/wet weight * 100%.

2.9. Brain infarct volume

The brain samples were cut into 5 slices at 2 mm intervals using a vibratome. The sections were incubated with 0.1 % TTC for 20 min at 37 °C in a dark room. After fixation in a 10% buffered formalin solution, images of the sections were captured using a digital camera.

The infarct volume was quantified from digitized TTC-stained brain sections using ImageJ software. The total infarct area (pale/white region) and the total hemispheric area for both the ipsilateral and contralateral sides were measured in each section. To correct for the confounding effect of cerebral edema, the infarct volume was calculated using the following standard formula:

Corrected Infarct Volume = [Infarct Area - (Ipsilateral Hemisphere Area - Contralateral Hemisphere Area)] × Section Thickness

2.10. Western blotting

After behavioral testing, the rats were sacrificed, brain cortex samples were removed and snap frozen in liquid nitrogen and kept at 80 °C. Next, after homogenizing the specimens in RIPA lysis buffer (Santa Cruz Biotechnology, USA) and centrifugation at 15,000g at 4 °C for 20 min, the supernatant was collected and the protein concentration measured by a BCA protein assay kit. After separation of equal protein samples by SDS-PAGE, they were transferred onto PVDF membranes and incubated with the primary antibodies include Anti-TLR4 (Cat No: ab217274, abcam), Anti-IL-1beta (Cat No: ab254360, abcam), Anti-IL-18 (Cat No: ab191860, abcam), Anti-NLRP3 (Cat No: ab263899, abcam), Anti- NFKB (Cat No: ab16502, abcam), Anti- TNF-alpha (Cat No: ab307164, abcam), Anti- MYD88 (Cat No: ab219413, abcam), and anti-Bactin-loading control antibodies (Cat No: ab8227 ; Abcam) overnight at 4°C. On the following day, PVDF membranes were incubated with appropriate HRP-labeled secondary antibodies for 2h at room temperature. The chemiluminescent HRP Substrate (Millipore) was employed to visualize the immunoreactive bands. Alpha Ease®FC Imaging System was employed to quantify the band density. β-actin was used as the housekeeping control.

2.11. Nissl staining (NS)

NS was used to detect neuronal death based on a previous study (Hasseldam, Rasmussen et al. 2024). The tissues were fixed with 4% paraformaldehyde, embedded in paraffin, and sliced into 5 µm sections. The slides were treated with xylene and ethanol and then soaked in PBS with 0.05 % Tween-20. After incubation in 0.1 % cresyl violet acetate for 10 min and a short incubation in acetic acid and 95 % ethanol, they were rapidly dehydrated and mounted for visualization and photography.

Viable neurons in the cortex region were counted in Nissl-stained sections under a light microscope at [400x magnification]. Intact neurons with a clear nucleus, prominent nucleolus, and rich Nissl substance were considered viable, while shrunken cells with pyknotic nuclei were excluded. Counting was performed in three randomly selected, non-overlapping fields per region per animal using the ImageJ (version 1.47, National Institutes of Health). The results are expressed as the number of viable neurons per mm² to account for potential differences in the field of view. All counts were performed by two independent investigators who were blinded to the group assignments

2.12. Statistical analysis

Data were presented as mean ± SD. Multiple comparisons were done using one-way analysis of variance (ANOVA) followed by post hoc Tukey test (GraphPad Prism 8.0 software). Statistical significance was defined as P value less than 0.05. Three animals succumbed to complications following the induction of cerebral ischemia and were excluded from the study. To maintain the statistical power and a consistent group size, these animals were replaced.

3. Results

3.1. Characterization of Apelin13-Loaded Niosomes

The morphology and size distribution of the synthesized Apelin13-Loaded Niosomes were investigated using scanning electron microscopy (SEM). Image reveal that the nanocomplexes are predominantly spherical in shape. The particles exhibit a relatively uniform size distribution, with an average diameter of 110 nm. The negative zeta potential of -42 mV further indicates excellent colloidal stability, attributable to strong electrostatic repulsion between the particles.

DLS analysis showed that the average diameter of Nano-Apelin13 was about 110.2 nm (Figure 1B). UV-Vis spectra of niosomes, free Apelin13, and Nano-Apelin13 are shown in Figure 1C. Both absorption peaks of free Apelin13 and nio-

somes are seen in Nano-Apelin13. ATR-FTIR spectroscopy was used to confirm the successful loading of Apelin13 into the niosomes. The ATR-FTIR spectra of control niosomes and Nano-Apelin13 are shown in Figure 1D. The spectra of control (empty) niosomes showed a broad peak at 3471 cm1, for O–H bond stretching. The sharp peak at 1635 cm 1 was due to the aromatic domain and N–H bending vibrations and also carbonyl groups. The spectra of Nano-Apelin13 is exactly the same as of control niosomes with the addition of sharper peaks at 690 cm1 and 2355 cm 1 characteristic of aromatic rings (C–H bending) and CC stretching vibrations, respectively. (Figure 1D). A reduction in the intensity of the broad peaks at 3471 cm^1 was observed after the incorporation of Apelin13.

3.2. In vitro drug release

The release pattern of Apelin13 from Nano-Apelin13 is shown in Figure 2. Cumulative drug release reached 82.5% from the niosomes over 24 hours. The drug release profile exhibited a biphasic pattern with an initial burst release followed by sustained release. The burst release was 50% in the first 7 h, which was attributed to the release of non-entrapped or adsorbed drug on the surface of the niosome vesicles. This was followed by a sustained release phase over the remaining 24 hours. The sustained release phase can be attributed to the niosomal bilayer structure, requiring drug diffusion from the inner core across the lipid bilayer. In addition, the presence of cholesterol, which stabilizes the niosome bilayer membrane, contributed to the sustained release profile. This sustained drug release behavior could provide a long-lasting effect in the body while reducing the frequency of dosing.

3.3. Measurement of infarct size

The TTC staining showed a significant infarct size in the brains of rats in the CI/R compared to sham-operated rats. Although the infarct size was significantly reduced in CI/R rats treated with free Apelin13, treatment with Nano-Apelin13 demonstrated a more pronounced effect on reducing the infarct size (Figure 3).

3.4. Neurological function scores

As shown in Figure 4, normal neurological behavior without any deficits was observed in the sham rats. A significant increase in NSS as an index of neurological deficits was observed in the CI/R vs. sham. Compared to the CI/R group, CI/R rats treated with free Apelin13 and Nano-Apelin13 showed a significant improvement in neurological deficits. The extent of improvement in the Apelin13 group is significant vs. sham ($p<0.05$), but the amount of improvement in the Nano-Apelin13 group is not significant vs. sham.

3.5. Brain edema

Compared with the sham group, the BWC was higher in rats in CI/R (Figure 4). Nano-Apelin13 significantly decreased the BWC compared to the CI/R, but free Apelin13 did not significantly reduce edema significantly compared to the CI/R.

3.6. Expression of proteins in the TLR4/MyD88/NF-B pathway

The results of the western blots showed that CI/R induction increased the phosphorylation of NF-B and the expression of TLR4 and MyD88 vs. sham rats. Reduced phosphorylation of NF-B and lower expression of MyD88 was observed in free Apelin13 and Nano-Apelin13 groups, but these changes were more significant in the Nano-Apelin13. The levels of TLR4 decreased significantly in Nano-Apelin13 vs CI/R but not significantly in free Apelin13 (Figure 5A-C).

3.7. Expression of inflammatory cytokines

CI/R induction significantly increased the expression of TNF- and IL-1β, compared to the sham group. The free Apelin13 group showed significantly higher levels compared to the sham group while the increase in the Nano-Apelin13 group was not statistically significant compared to sham. Free Apelin13 failed to significantly reduce TNF- and IL-1β levels but Nano-Apelin13 significantly decreased amounts of TNF- and IL-1β versus the CI/R (Figure 6A-B).

3.8. Neuronal damage

The pathological changes in the rat cortex were investigated by Nissl staining (NS). Sham rats showed normal morphology and structure of neurons in the cortex area. Numerous shrunken nuclei and deeply stained pyramidal neurons in the neurons of the cortex region were observed in CI/R rats. The damage to rat cortical cells was reduced after treatment with Apelin13 ($p<0.05$) and Nano-Apelin13 ($p<0.01$), but the reduction was more pronounced in the Nano-Apelin13 group (Figure 7).

4. Discussion

In our present investigation, we found that the induction of MCAO produced a sizeable infarct volume, brain edema, nerve deficits, and neuronal loss in the cortex region. The 24-hour post-reperfusion time point was selected to specifically target the acute phase of ischemic injury. This early window is critical, as key pathological processes—including intense inflammatory response, oxidative stress, blood-brain barrier disruption, and the initiation of apoptosis—peak during this period. Our study was designed as a proof-of-concept investigation to determine the efficacy of our intervention in modulating these initial injury mechanisms. While longer-term studies are essential to assess functional recovery and are a clear goal for future research, the 24-hour endpoint allows for a clearer interpretation of the treatments direct effects on acute damage before significant spontaneous recovery and increased variability in the transient MCAO model confound the results. Both free Apelin13 and Nano-Apelin13 could markedly reduce the size of the cerebral infarct area, neurological deficit scores and cell death in the cortex region. However, Nano-apelin13 showed a more powerful effect on these

markers compared to free Apelin13, with a more substantial reduction in the Nano-Apelin13 group. Regarding the reduction in the expression of MyD88/NF-B proteins, despite a reduction in both groups treated with free Apelin13 or Nano-Apelin13 compared to the CI/R group, the Nano-Apelin13 group was almost restored to the level of the sham group. Regarding the reduction of TLR4 expression, Nano-Apelin13 was able to produce a significant reduction compared to the CI/R group, but the free Apelin13 group showed no significant reduction. Nano-Apelin13 significantly reduced brain edema compared to the CI/R group, but free Apelin13 did not significantly reduce edema. Regarding the reduction of inflammatory cytokines, Nano-Apelin13 significantly reduced both inflammatory factors almost to the level of the sham group, but free Apelin13 did not produce a significant reduction compared to CI/R.

The MCAO model is accepted as a classic stroke animal model for testing new therapeutic approaches, and exploring their molecular mechanisms for possible use in patients (Zhou, Chen et al. 2019, Barthels and Das 2020) . The pathophysiology of IS is complex and involves various biochemical processes, such as oxidative stress and inflammatory reactions (Wu, Yiang et al. 2018). Among various types of molecular mechanisms, inflammatory responses are one of the most important in CI/R injury leading to accelerated death of brain cells (Pundik, Xu et al. 2012).

TLR4 acts as a mediator of inflammation and damage in different types of I/R models, especially in CI/R (Wang, Ge et al. 2013). During ischemia, the release of damage-associated molecule pattern proteins (DAMPs) such as HMGB1 and S100B from the site of injury results in the activation of TLR4 (Yu, Wang et al. 2006). Activated TLR4 is capable of accelerating the phosphorylation of NF-κB in a MyD88-related process, which in turn initiates the production of inflammatory cytokines like TNF-, IL-1β, and IL-6 (Zhang, Peng et al. 2017, Sun, Yang et al. 2021). In our present investigation, it was found that induction of MCAO increased the activity of the TLR4/MyD88/NF-B axis, but this activation was inhibited by both free Apelin13 and Nano-Apelin13.

Our findings are consistent with previous investigations showing the protective effects of free Apelin13 by suppression of the TLR4 and NLRP3 axis or the NF-κB pathway inhibiting NLRP3 inflammasome activation (Luo, Liu et al. 2018, Zhang, Chen et al. 2018). NF-κB is a master regulator of different types of cellular processes and plays a crucial role in neuronal damage, cell death, and inflammation during ischemia (Yan, Chen et al. 2021). The neuronal loss caused by ischemia is associated with excessive generation of proinflammatory and reduced amounts of anti-inflammatory cytokines (IL-10) (Pinsky, Goonewardena et al. 2016). In our present investigation, we observed that the neuronal loss following MCAO induction was improved by both free Apelin13 and Nano-Apelin13. Our results are in agreement with a previous study showing that free Apelin13 was capable of reducing the damage caused by IS by attenuating neuronal damage and infarct size (Shao, Dou et al. 2021). While the present study provides compelling evidence for the efficacy of Nano-Apelin13 in mitigating neuroinflammation following cerebral ischemia/reperfusion injury, primarily through the suppression of the pro-inflammatory TLR4/MyD88/NF-κB axis and its downstream effectors TNF- and IL-1β, it is important to acknowledge its limitations. A key aspect not investigated here is the potential modulation of anti-inflammatory pathways. The overall inflammatory balance post-stroke is critically determined by the equilibrium between pro-inflammatory and anti-inflammatory mediators, such as the key regulatory cytokine IL-10. Future studies are warranted to determine whether the potent anti-inflammatory effects of Nano-Apelin13 observed in this study are coupled with a concomitant upregulation of anti-inflammatory cytokines, which would indicate a more comprehensive shift in the immune response towards a reparative state. Elucidating the impact of Nano-Apelin13 on the polarization of microglia and infiltrating macrophages towards an anti-inflammatory (M2) phenotype represents a crucial next step in fully characterizing its immunomodulatory potential and therapeutic promise.

The ability of Nano-Apelin13 to suppress the activity of TLR4/MyD88/NF-kB pathway and improve the damage caused by CI/R was more pronounced than free Apelin13. The niosomes were shown to be able to improve the efficiency of Apelin13 as a neuroprotective agent. The unique properties of niosomes, including extending the circulation time of the entrapped drug, modifying its organ distribution and metabolic stability, their capacity to load drugs with limited solubility in water, and their low toxicity, have made them good drug delivery vehicles (Pires, Paiva-Santos et al. 2023) (Bhardwaj, Tripathi et al. 2020, Kushnazarova, Mirgorodskaya et al. 2021) (Hameed, Khan et al. 2024). The niosomes used in this study contained a combination of non-ionic surfactant and cholesterol. Studies have reported the use of nonionic surfactants in the delivery of anticancer drugs (Li, Sun et al. 2014, Ge, Wei et al. 2019), steroids (Shah, Goodyear et al. 2021), and HIV protease inhibitors (Kumar and Rajeshwarrao 2011), and antidiabetics drugs (Sankhyan and Pawar 2013) because of improved absorption and targeting. Non-ionic surfactants with no charge on the polar head groups can be used in drug delivery carriers to provide controlled drug release, along with improved duration and location. Cholesterol can affect the membrane permeability and stiffness, improve drug entrapment efficiency, allow rehydration of desiccated niosomes, improve the stability, storage conditions, and lessen toxicity. In addition to protecting drugs from premature degradation, cholesterol also inhibits unwanted immunological effects and improves the pharmacology (Barthels and Das 2020). An interesting observation in our study was the modest effects exhibited by the empty niosome group in some outcome measures compared to the pure control. While significantly lower than the group receiving the drug-loaded niosomes, this activity warrants con-

sideration. The components of niosomes, particularly non-ionic surfactants, are known to interact with biological membranes, potentially modulating fluidity and cellular signaling (Bashkeran, Kamaruddin et al. 2023). Furthermore, the lipid-based structure itself might exhibit mild anti-inflammatory or cytoprotective properties. It is also plausible that the niosomes act as a biological 'primer,' subtly altering the cellular environment and enhancing resilience to ischemic stress. Nonetheless, the pronounced superiority of the drug-loaded niosomes unequivocally demonstrates that the therapeutic efficacy is primarily driven by the active pharmaceutical ingredient, with the niosome system serving to enhance its delivery and potency.

5. Limitations

Although rat model offered important evidence regarding the anti-inflammatory potential of niosomal Apelin-13, species-related differences in immune and physiological responses may restrict the generalization of these findings to humans. Therefore, additional investigations using human-based experimental models and clinical studies are necessary to validate the translational relevance of the results. Additionally, while niosomes enhances the delivery of Apelin-13, the complete biodistribution pattern and the long-term stability of the formulation in various physiological conditions were not fully characterized. Future research should involve advanced imaging techniques to track the real-time distribution of these nanocarriers.

6. Conclusions

We showed that gradual release of the endogenous peptide Apelin13from niosomes enhanced its therapeutic efficacy against cerebral ischemia/reperfusion injury in a rat MCAO model. The observed reduction in inflammation and brain edema may be attributed to improved drug bioavailability and stability provided by the niosomal formulation, leading to enhanced neuroprotective effects. Moreover, our findings suggested that the neuroprotective effects of Apelin13 released from niosomes could be attributed to inhibition of TLR4/MyD88/NF-B axis.

7. Declarations

7.1. Acknowledgments

The authors would like to sincerely thank all those who contributed to this research, particularly the laboratory staff, for their technical assistance and continuous support during the experimental procedures.

7.2. Authors' contributions

F.R, N.A participated in the design and interpretation of the study, data analysis, and the review of the manuscript. E.K-J, S.N-M and F.R conducted the experiment and collected the tissue and was responsible for the data analysis. E.K-J performed histopathological analyses. E.K-J and F.R wrote the manuscript, M.R.H critically revised the first draft, all authors reviewed, read, and approved the article.

7.3. Funding/Support

This work was funded by the Vice Chancellor of Research, Iran University of Medical Sciences, Grant number: (26220-4-2-1402).

7.4. Competing interests

The authors have no relevant financial or nonfinancial interests to disclose.

7.5. Ethics approval and consent to participate

All protocols were approved by Ethical Committee of Iran University of Medical Sciences, Tehran, Iran (Ethics code: IR.IUMS.FMD.REC.1402.083).

7.6. Consent for publication

All authors agree to publish article in the present form

7.7. Availability of data and materials

The data that support the findings of this study are available from the corresponding author upon reasonable request.

7.8. Using artificial intelligence chatbots

None.

References

1. Barthels, D. and H. Das (2020). "Current advances in ischemic stroke research and therapies." Biochimica et Biophysica Acta (BBA)-Molecular Basis of Disease 1866(4): 165260.
2. Barton, G. M. and R. Medzhitov (2003). "Toll-like receptor signaling pathways." Science 300(5625): 1524–1525.
3. Bashkeran, T., et al. (2023). "Niosomes in cancer treatment: A focus on curcumin encapsulation." Heliyon 9(8).
4. Behrouzifar, S. and H. Esmaily (2024). "The biological efficacy of Apelin against focal transient cerebral ischemia–reperfusion injury. A systematic review and meta-analysis of animal studies." Brain Research 1833: 148887.
5. Bhardwaj, P., et al. (2020). "Niosomes: A review on niosomal research in the last decade." Journal of Drug Delivery Science and Technology 56: 101581.
6. Feigin, V. L., et al. (2021). "Global, regional, and national burden of stroke and its risk factors, 1990–2019: a systematic analysis for the Global Burden of Disease Study 2019." The Lancet Neurology 20(10): 795–820.
7. Feske, S. K. (2021). "Ischemic stroke." The American journal of medicine 134(12): 1457–1464.
8. Ge, X., et al. (2019). "Advances of Non-Ionic Surfactant Vesicles (Niosomes) and Their Application in Drug Delivery." Pharmaceutics 11(2).

9. Hameed, H., et al. (2024). "Liposomes like advanced drug carriers: from fundamentals to pharmaceutical applications." Journal of Microencapsulation 41(6): 456–478.
10. Hasseldam, H., et al. (2024). "N-acetyl aspartate levels early after ischemic stroke accurately reflect long-term brain damage." Heliyon 10(2).
11. Kleindorfer, D. O., et al. (2021). "2021 guideline for the prevention of stroke in patients with stroke and transient ischemic attack: a guideline from the American Heart Association/American Stroke Association." stroke.
12. Kumar, G. P. and P. Rajeshwarrao (2011). "Nonionic surfactant vesicular systems for effective drug delivery—an overview." Acta Pharmaceutica Sinica B 1(4): 208–219.
13. Kushnazarova, R. A., et al. (2021). "Niosomes modified with cationic surfactants to increase the bioavailability and stability of indomethacin." Russian Chemical Bulletin 70(3): 585–591.
14. Li, C., et al. (2014). "Novel designed polyoxyethylene nonionic surfactant with improved safety and efficiency for anticancer drug delivery." International Journal of Nanomedicine 9(null): 2089–2100.
15. Longa, E. Z., et al. (1989). "Reversible middle cerebral artery occlusion without craniectomy in rats." stroke 20(1): 84–91.
16. Luo, Q., et al. (2018). "Apelin protects against sepsis-induced cardiomyopathy by inhibiting the TLR4 and NLRP3 signaling pathways." Int J Mol Med 42(2): 1161–1167.
17. Mendelson, S. J. and S. Prabhakaran (2021). "Diagnosis and management of transient ischemic attack and acute ischemic stroke: a review." Jama 325(11): 1088–1098.
18. Pinsky, D., et al. (2016). "Inflammatory Disequilibrium in Stroke." Circulation Research 119(1): 142–158.
19. Pires, P. C., et al. (2023). "Liposome-Derived Nanosystems for the Treatment of Behavioral and Neurodegenerative Diseases: The Promise of Niosomes, Transfersomes, and Ethosomes for Increased Brain Drug Bioavailability." Pharmaceuticals 16(10): 1424.
20. Powers, W. J., et al. (2019). "Guidelines for the early management of patients with acute ischemic stroke: 2019 update to the 2018 guidelines for the early management of acute ischemic stroke: a guideline for healthcare professionals from the American Heart Association/American Stroke Association." stroke 50(12): e344–e418.
21. Pundik, S., et al. (2012). "Reperfusion brain injury: focus on cellular bioenergetics." Neurology 79(13_supplement_1): S44–S51.
22. Riya, S., et al. (2022). "An overview on Niosomes: Novel Pharmaceutical drug delivery system." Journal of drug delivery & therapeutics 12: 171–177.
23. Sankhyan, A. and P. K. Pawar (2013). "Metformin loaded non-ionic surfactant vesicles: optimization of formulation, effect of process variables and characterization." DARU Journal of Pharmaceutical Sciences 21(1): 7.
24. Schneider, S., et al. (2021). "Determinants of long-term health-related quality of life in young ischemic stroke patients." Journal of Stroke and Cerebrovascular Diseases 30(2): 105499.
25. Shah, P., et al. (2021). "Nanostructured Non-Ionic Surfactant Carrier-Based Gel for Topical Delivery of Desoximetasone." Int J Mol Sci 22(4).
26. Shao, Z.-Q., et al. (2021). "Apelin-13 inhibits apoptosis and excessive autophagy in cerebral ischemia/reperfusion injury." Neural Regeneration Research 16(6): 1044–1051.
27. Sun, J.-H., et al. (2021). "Gentianella acuta prevents acute myocardial infarction induced by isoproterenol in rats via inhibition of galectin-3/TLR4/MyD88/NF-B inflammatory signalling." Inflammopharmacology 29(1): 205–219.
28. Wang, L., et al. (2022). "Nrf2 regulates oxidative stress and its role in cerebral ischemic stroke." Antioxidants 11(12): 2377.
29. Wang, Y., et al. (2013). "TLR2 and TLR4 in the brain injury caused by cerebral ischemia and reperfusion." Mediators of inflammation 2013(1): 124614.
30. Wang, Z., et al. (2023). "Shell-sheddable polymeric micelles alleviate oxidative stress and inflammation for enhanced ischemic stroke therapy." Nano Letters 23(14): 6544–6552.
31. Wu, M.-Y., et al. (2018). "Current mechanistic concepts in ischemia and reperfusion injury." Cellular Physiology and Biochemistry 46(4): 1650–1667.
32. Xu, S., et al. (2022). "Nano-liposomal encapsulation-delivered apelin-13 attenuates Ev71 infection-induced neurodegeneration by modulating Il-6 and Tlr7." Journal of Modern Nanotechnology 2(1).
33. Yafasova, A., et al. (2021). "Time to thrombolysis and long-term outcomes in patients with acute ischemic stroke: a nationwide study." stroke 52(5): 1724–1732.
34. Yan, Z., et al. (2021). "Neuroprotective Function of TNFAIP3 Interacting Protein 2 Against Oxygen and Glucose Deprivation/Reoxygenation-Induced Injury in Hippocampal Neuronal HT22 Cells Through Regulation of the TLR4/MyD88/NF-κB Pathway." Neuropsychiatric Disease and Treatment 17(null): 2219–2227.
35. Yang, C., et al. (2021). "Analgecine regulates microglia polarization in ischemic stroke by inhibiting NF-κB through the TLR4 MyD88 pathway." International Immunopharmacology 99: 107930.
36. Yu, M., et al. (2006). "HMGB1 SIGNALS THROUGH TOLL-LIKE RECEPTOR (TLR) 4 AND TLR2." Shock 26(2): 174–179.
37. Zhang, H., et al. (2018). "Apelin-13 Administration Protects Against LPS-Induced Acute Lung Injury by Inhibiting NF-kappaB Pathway and NLRP3 Inflammasome Activation." Cell Physiol Biochem 49(5): 1918–1932.
38. Zhang, J. J., et al. (2017). "Dexmedetomidine preconditioning may attenuate myocardial ischemia/reperfusion injury by down-regulating the HMGB1-TLR4-MyD88-

NF-small ka, CyrillicB signaling pathway." PLoS One 12(2): e0172006.
39. Zhang, Y., et al. (2023). "Neuroprotective roles of apelin-13 in neurological diseases." Neurochemical Research 48(6): 1648–1662.
40. Zhou, K., et al. (2019). "Atractylenolide III ameliorates cerebral ischemic injury and neuroinflammation associated with inhibiting JAK2/STAT3/Drp1-dependent mitochondrial fission in microglia." Phytomedicine 59: 152922.

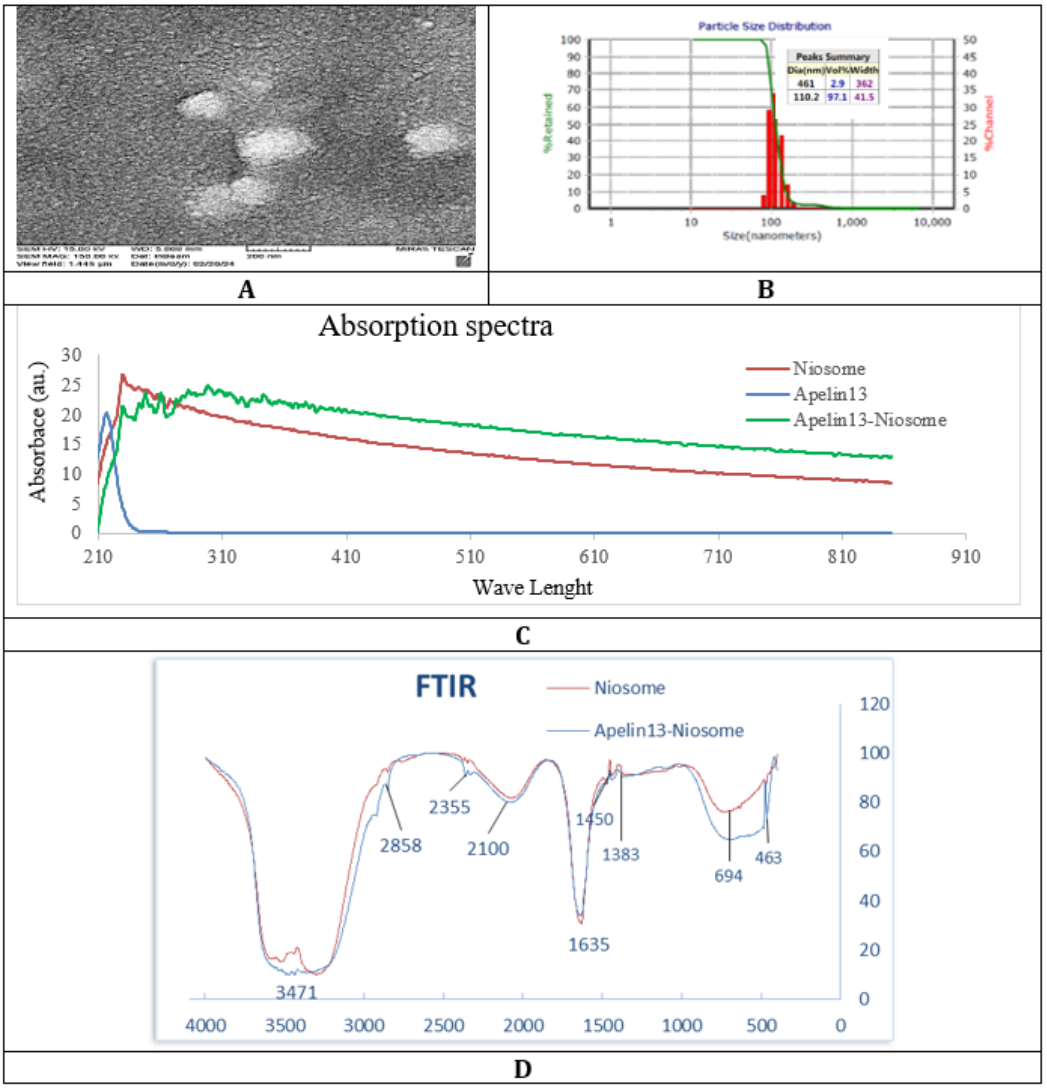

Figure 1: Characterization of nanocomplex. A) Scanning electron microscopy (SEM) image of nanocomplex, B) Dynamic light scattering (DLS) results for dynamic size of Nano-Apelin13; C) Ultraviolet-visible spectroscopy (UV-Vis) spectra of Apelin13, niosomes and Nano-Apelin13 complex; D) Fourier-transform infrared spectroscopy (FTIR) spectra of niosomes and Nano-Apelin13.

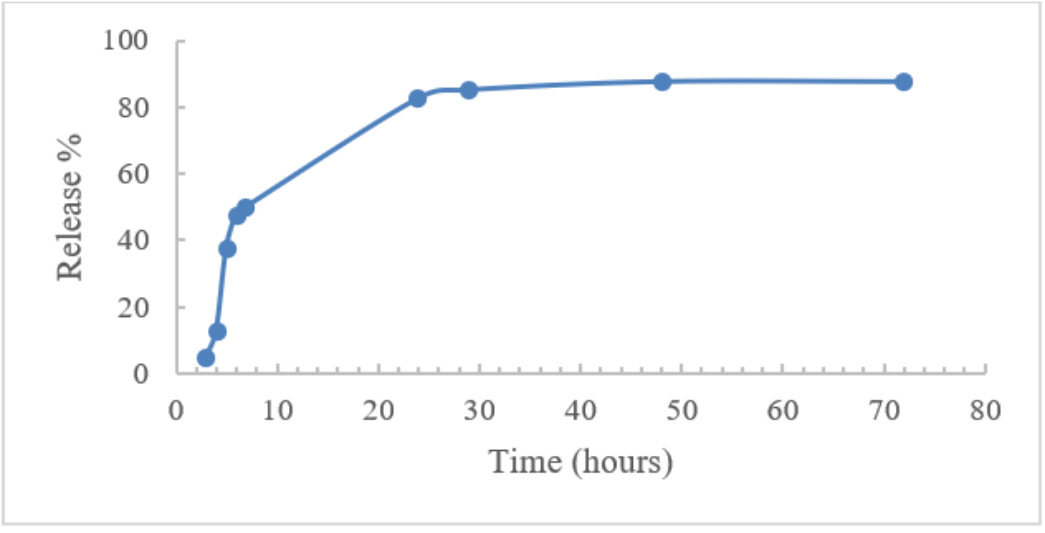

Figure 2: Drug release pattern. % of drug release from Nano-Apelin13

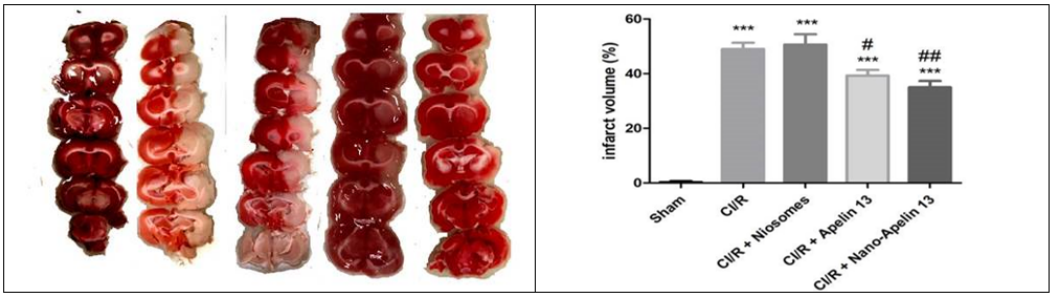

Figure 3: Infarct size following cerebral ischemia–reperfusion (CI/R). Values are mean ± standard deviation (SD) (***p<0.001 vs. sham, #p<0.05 and ##p<0.01 vs. CI/R and niosomes groups), n=4 for each group.

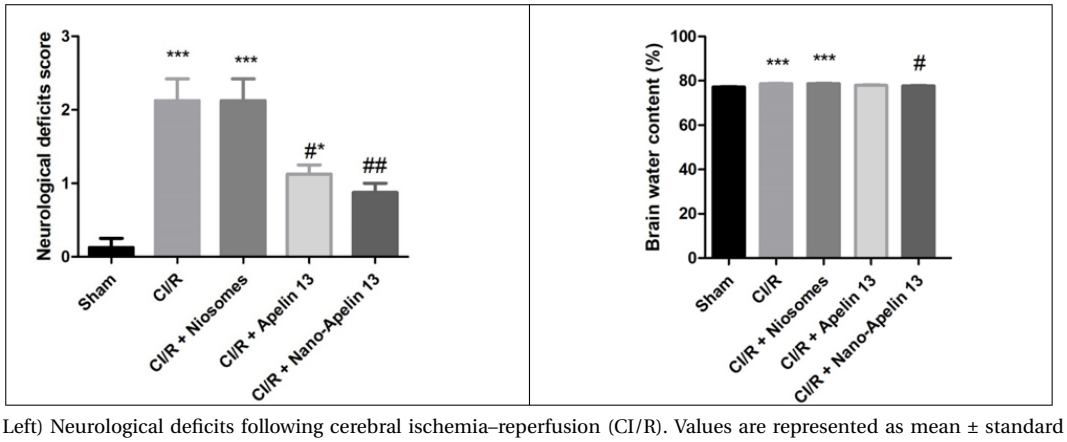

Figure 4: Left) Neurological deficits following cerebral ischemia–reperfusion (CI/R). Values are represented as mean ± standard deviation (SD) (*p<0.05 and ***p<0.001 vs. sham, #p<0.05 and ##p<0.01 vs. CI/R groups), n=4 for each group. Right) Measurement of brain water content following CI/R. Values are mean ± SD (*p<0.05 and ***p<0.001 vs. sham, #p<0.05 and ##p<0.01 vs. CI/R groups), n=4 for each group.

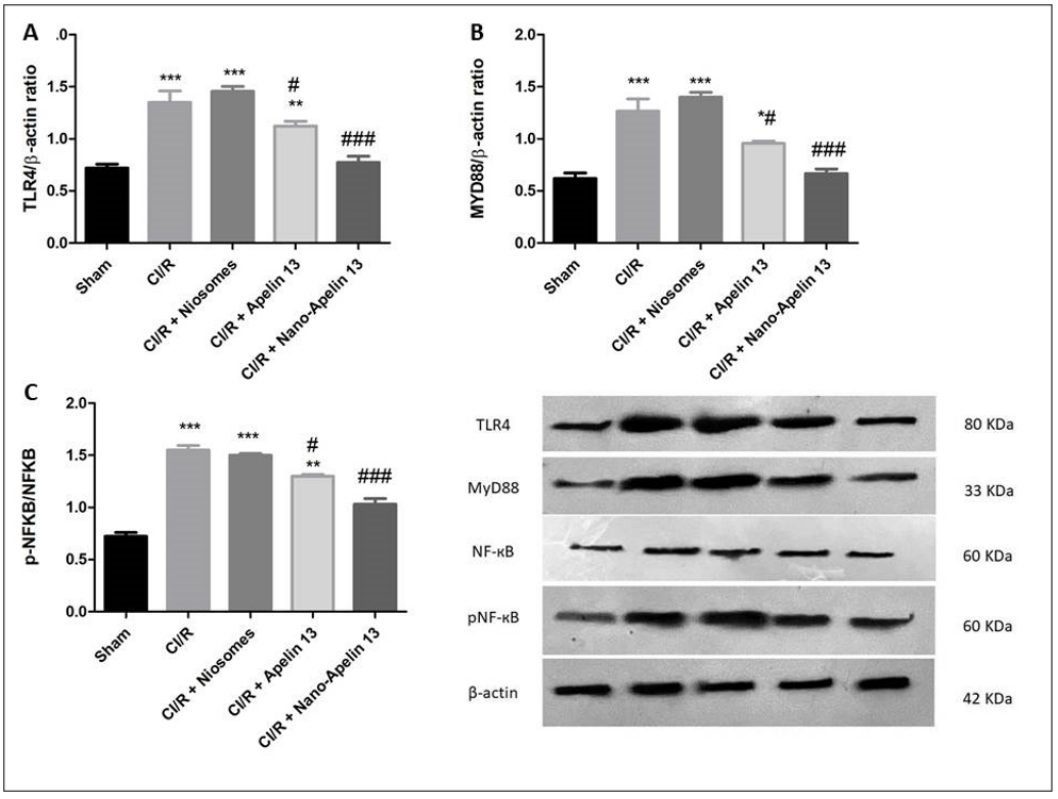

Figure 5: Western blot analysis of the Toll-Like Receptor 4 (TLR4)/Myeloid Differentiation Primary Response 88 (MyD88)/Nuclear Factor kappa-light-chain-enhancer of activated B cells (NF-κB) signaling axis proteins. Expression levels of (A) Toll-Like Receptor 4 (TLR4), (B) Myeloid Differentiation Primary Response 88 (MyD88), and © Nuclear Factor kappa-light-chain-enhancer of activated B cells (NF-κB) following cerebral ischemia/reperfusion (CI/R) injury in different experimental groups. Data are presented as mean ± standard deviation (SD). *p < 0.05, **p < 0.01, and ***p < 0.001 compared with the sham group; #p < 0.05 and ###p < 0.001 compared with the cerebral ischemia/reperfusion (CI/R) group. Sample size: n = 4 per group.

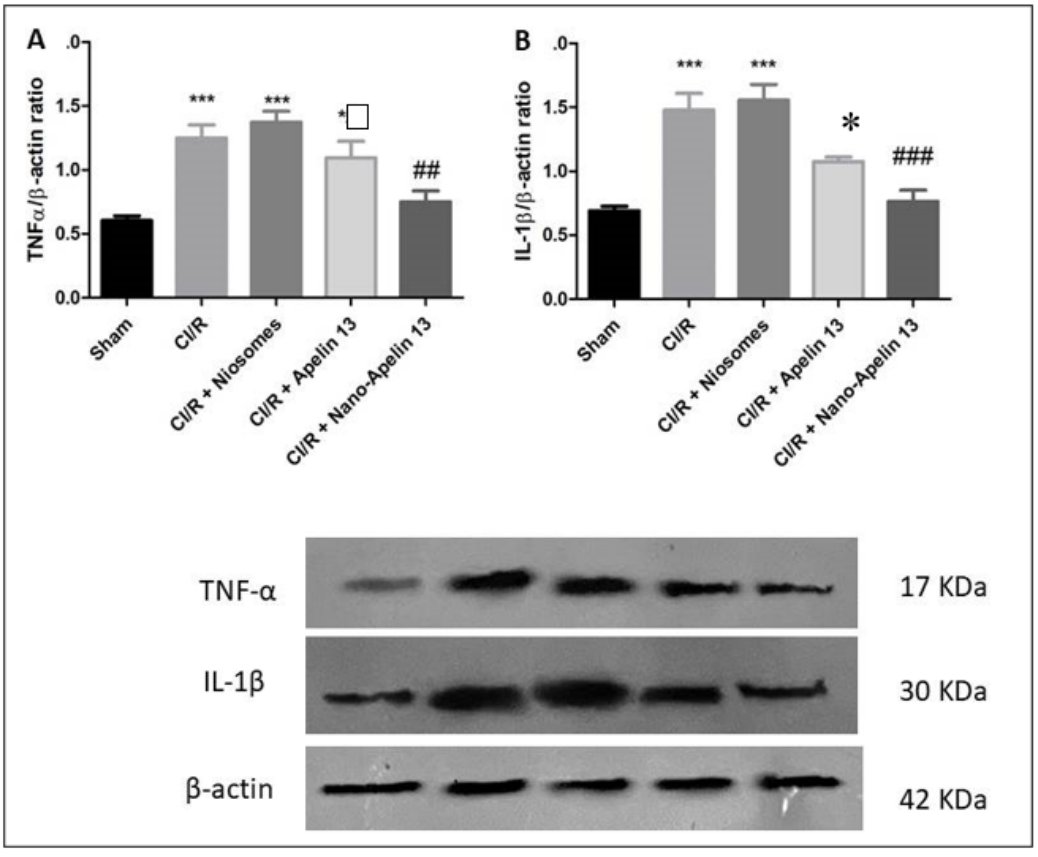

Figure 6: Western blot analysis of pro-inflammatory cytokines. Expression of (A) Tumor Necrosis Factor-alpha (TNF-) and (B) Interleukin-1 beta (IL-1β) following cerebral ischemia/reperfusion (CI/R) injury in different experimental groups. Data are presented as mean ± standard deviation (SD). *p < 0.05 and ***p < 0.001 compared with the sham group; #p < 0.05, ##p < 0.01, and ###p < 0.001 compared with the cerebral ischemia/reperfusion (CI/R) group. Sample size: n = 4 per group.

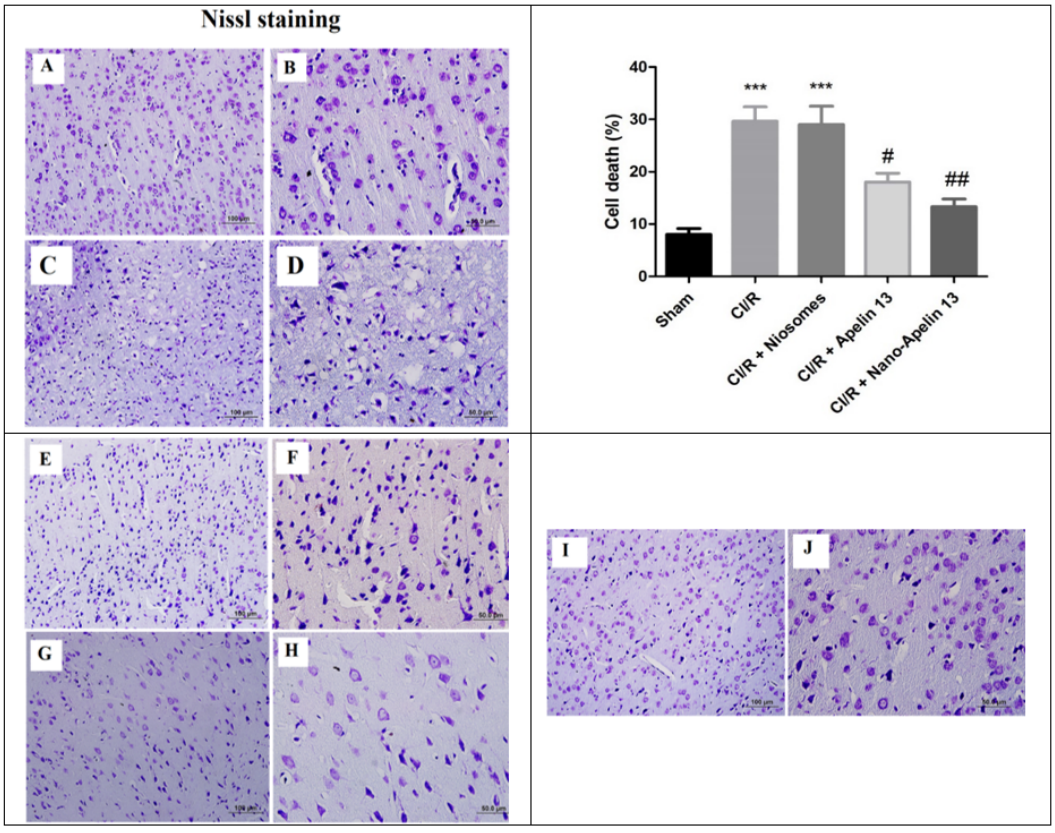

Figure 7: Assessment of neuronal damage and cell death following cerebral ischemia/reperfusion (CI/R) injury in different experimental groups. Representative images: (A, B) sham group; (C, D) cerebral ischemia/reperfusion (CI/R) group; (E, F) niosome-treated group (niosomes are non-ionic surfactant-based vesicular nanocarriers); (G, H) Apelin-13-treated group (Apelin-13 is a 13-amino-acid bioactive peptide of the apelin family); and (I, J) nano-Apelin-13-treated group (nanoparticle-encapsulated Apelin-13). Data are presented as mean ± standard deviation (SD). ***$p < 0.001$ compared with the sham group; #$p < 0.05$ and ##$p < 0.01$ compared with the cerebral ischemia/reperfusion (CI/R) group. Sample size: n = 4 per group.